P14R.7 RADAR OBSERVATIONS OF A NEGATIVE CLOUD-TO-GROUND STORM OBSERVED DURING STEPS

Sarah A. Tessendorf* and Steven A. Rutledge
Colorado State University, Fort Collins, Colorado

1. INTRODUCTION

The Severe Thunderstorm Electrification and Precipitation Study (STEPS; Lang et al. 2004) field campaign took place between 17 May 2000 and 20 July 2000 in eastern Colorado and western Kansas. STEPS research aims to identify relationships between storm dynamics, microphysics, and electrification in storms on the High Plains, where a high percentage of storms that produce anomalous positive cloud-to-ground (CG) lightning have been documented (Carey et al. 2003). This study presents observations of a *negative* CG-producing storm observed during STEPS, and compares it with the 29 June 2000 positive CG-producing storm (MacGorman et al. 2005, Tessendorf et al. 2005, Wiens et al. 2005).

On 19 June 2000, a multicellular storm system produced abundant intra-cloud (IC) lightning but only a few CG strikes, which were predominantly of negative polarity. Peak surface winds of 33 m s^{-1} and pea-sized hail were documented by surface observations. The storm presented herein developed southwest of the CSU-CHILL radar around 2300 UTC and traveled east-northeast toward the CSU-CHILL radar. After passing over the CSU-CHILL radar around 0030 UTC, the storm began to dissipate while a new group of cells developed just west of Goodland, KS. These new cells rapidly evolved and propagated to the northeast through the STEPS domain. This portion of the storm dissipated northeast of Goodland, KS just after 0200 UTC (20 June). This study provides a preliminary analysis of the observations from this storm system.

2. DATA AND METHODS

Instrumentation and observing systems operated during STEPS that are most central to this study included three S-Band Doppler radars (two of which were polarimetric research radars) for mapping the three-dimensional structure of precipitation and storm winds, the National Lightning Detection Network (NLDN; Cummins et al. 1998), and the 3-D Lightning Mapping Array (LMA; Rison et al. 1999) operated by New Mexico Institute of Mining and Technology.

2.1 Radar data processing

The CSU-CHILL polarimetric Doppler radar, the National Center for Atmospheric Research (NCAR) S-Pol polarimetric Doppler radar, and the Goodland, Kansas National Weather Service (NWS) WSR-88D radar (KGLD) comprised the triple-Doppler radar network used to take the radar measurements. The three radars were arranged in a rough equilateral triangle with approximately 60-km sides (Fig. 1).

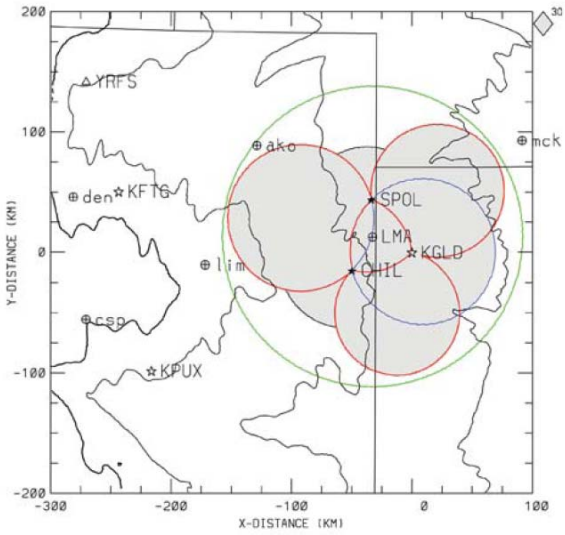

Figure 1. Nominal areas of coverage (shading) by the triple-Doppler radar network (from Lang et al. 2004).

The dual linear polarization capability, on the CSU-CHILL and NCAR S-Pol radars, enables the radar to detect hydrometeor shape and size that, when combined with air temperature, can be used to infer hydrometeor type.

Wind field syntheses were completed for 27 volume scans during the period 2318 (19 June)-0213 (20 June). The radar data were interpolated onto a Cartesian grid using NCAR's Sorted Position Radar INTerpolator (SPRINT).

* *Corresponding author address*: Sarah A. Tessendorf, Colorado State Univ., Dept. of Atmospheric Science, Fort Collins, CO 80523-1371; e-mail: saraht@atmos.colostate.edu

Grid resolution was 0.5 km in both the horizontal and vertical directions. After the grid interpolation, the velocity data were globally unfolded by means of NCAR's Custom Editing and Display of Reduced Information in Cartesian Space (CEDRIC) software (Mohr et al. 1986). The three dimensional wind fields were computed using the radial velocities from S-Pol and KGLD between 2318-0059 UTC[1] and from S-Pol and CHILL between 0106-0213 UTC. The speed and direction of storm movement were calculated and used for the advection parameters. The vertical velocities were obtained using a variational integration of the continuity equation (O'Brien 1970).

The polarimetric data were edited to eliminate noise, clutter, and suspect data following the methods outlined in Ryzhkov and Zrnic (1998). The processed data were then gridded in the same manner as described above. A fuzzy-logic hydrometeor classification scheme, (hereafter FHC), adapted from Liu and Chandrasekar (2000) and Straka et al. (2000), was implemented for the Cartesian gridded data to estimate bulk hydrometeor types within the storm (Tessendorf et al. 2005). Hydrometeor echo volumes were also calculated for each radar scan time by multiplying the number of grid points (N) that satisfied the FHC category of interest by the volume of a grid box (0.125 km^3). Time series of the polarimetric results and the vertical motion estimates were then compared.

2.2 Lightning data processing

The New Mexico Tech LMA measures the time and three-dimensional location of very high frequency (VHF) radiation sources emitted by lightning discharges. For a given lightning flash, the LMA may locate hundreds to thousands of such sources resulting in detailed maps of the total lightning activity. To interpret these data, we use the bi-directional discharge model (Kasemir 1960, Mazur and Ruhnke 1993). This model suggests that flashes initiate in strong electric field between regions of opposite net charge, and then propagate bi-directionally into the two charge regions. Keeping in mind that the negative breakdown component of a lightning flash is noisier at VHF, which makes it more frequently detected by the LMA than the positive breakdown component, we can infer charge regions based on the location of flash initiation, its temporal evolution, and the relative number of LMA sources on either side of the flash initiation location. Furthermore, we also assume that negative breakdown passes through regions of net positive charge, and vice versa. For example, if the LMA sources from a flash initially propagate upward, we infer that the flash is initiating between net positive and negative charge regions and then it travels into the region of net positive charge that resides above the region of net negative charge. Typically those sources that reside below the height of flash initiation are from the negative charge region, and are often much fewer in number than those in the positive region. To determine total (CG plus IC) flash rates from the LMA data, we used an algorithm developed at New Mexico Tech (Thomas et al. 2003) that sorts the LMA sources into discrete flashes.

3. OBSERVATIONS

3.1 Overview

A dry line had set up along the Colorado-Kansas border by 1000 UTC the morning of 19 June 2000 with surface dew points in the upper 50's °F to low 60's °F to the east of the dry line, and in the mid-40's °F to the west of the line. A 500 mb trough was situated over Utah, giving way to mid-to-upper level southwesterly flow into the STEPS region. Surface temperatures were in the mid-to-upper 80's °F, but due to a very dry boundary layer the CAPE was marginal (566 J kg^{-1} in Fig. 2 and even less in other MGLASS soundings). Surface winds were relatively weak, but mostly southerly east of the dry line, and westerly west of the dry line. A ridge in surface equivalent potential temperature was situated in north-central Kansas and into south-central Nebraska, further east of the STEPS domain.

By 2200 UTC, a multicellular storm system developed near Colorado Springs, CO and was traveling to the northeast toward the STEPS domain. A new cell developed southwest of the CSU-CHILL radar around 2300 UTC and was targeted by the STEPS radar network (Fig. 3; hereafter Storm A). By the beginning of the analysis period at 2318 UTC, this storm was already producing IC and mostly negative CG lightning. The storm rapidly evolved while propagating to the northeast and was in its mature

[1] Except at 0019 UTC, when S-Pol and CHILL were used in the absence of a KGLD volume scan near that time.

phase by 0000 UTC. It passed over the CSU-CHILL radar near 0030 UTC and dissipated shortly thereafter. Near the time of its dissipation, another group of cells was developing west of KGLD (hereafter Storm B). These cells quickly began producing IC and mostly negative CG lightning, as they propagated to the northeast. The cells eventually merged into an elongated storm by 0122 UTC, and between 0124-0154 UTC there were three reports[2] of severe winds greater than 50 kts associated with this storm, the latter of which was as high as 65 kts. Storm B's peak in maximum updraft and graupel echo volume was observed around 0200 UTC. Shortly after this time, the storm quickly dissipated, however, CG flash rates peaked right before dissipation at 0208 UTC.

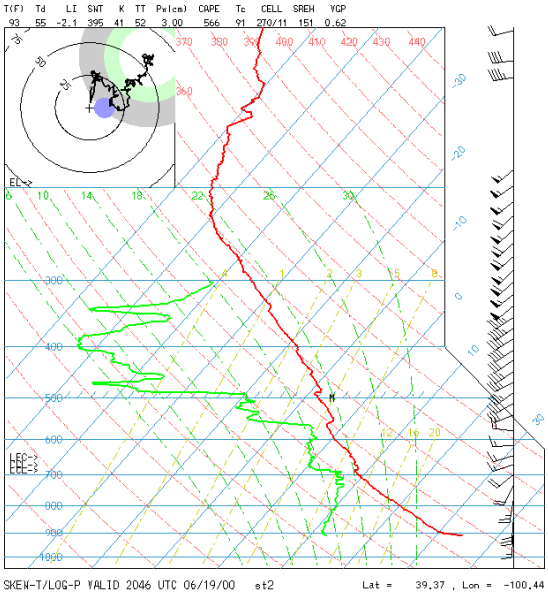

Figure 2. MGLASS thermodynamic sounding taken near Colby, Kansas at 2046 UTC 19 June 2000.

3.2 Time series

Using the maximum updraft curve illustrated in Fig. 4, we define phases in each storm's lifecycle, which we will refer to later in the text. Between the beginning of the analysis period and approximately 0000 UTC, Storm A was in a developing phase. The maximum updraft in this phase was around 10 m s^{-1} (Fig. 4). After this point, the maximum updraft began to increase indicating the beginning of Storm A's mature phase. The maximum updraft reached 15 m s^{-1} during this phase at 0025 UTC (Fig. 4). The maximum downdraft also peaked at 12 m s^{-1} during this phase (not shown). After 0030 UTC, Storm A entered its dissipating phase as the maximum updraft began to decline to around 6 m s^{-1} (Fig. 4). The maximum downdraft remained near 10 m s^{-1} into the dissipating phase (not shown). Storm A had essentially dissipated by 0052 UTC. At 0044 UTC, Storm B began to develop and was targeted by the STEPS radar network. It remained in its developing phase until 0142 UTC when its maximum updraft quickly increased to near 10 m s^{-1} (Fig. 4). Storm B's mature phase (from ~0142-0208 UTC) was fairly short-lived, and had a brief maximum updraft of 18 m s^{-1} just after 0200 UTC ((Fig. 4). The maximum downdraft in Storm B peaked at 11 m s^{-1} during its mature phase, and was also short-lived (not shown). Storm B rapidly dissipated after 0208 UTC. The updraft volume greater than 10 m s^{-1} (hereafter, UV10) was very small in these storms. The only times when UV10 was apparent were in the mature phases of each storm.

Graupel was already detected at the beginning of the analysis period in Storm A by the FHC algorithm, and graupel echo volume (hereafter, graupel EV) continually increased until 0025 UTC in Storm A's mature phase (Fig. 5). After this point, graupel EV dramatically declined[3] and then increased again until it reached its greatest peak in the mature phase of Storm B at 0155 UTC. Most of the graupel EV was centered around 6 km MSL (corresponding to a temperature near –10 °C) until around 0030 UTC (Fig. 4). After that time, during the dissipating phase of Storm A, the center of the graupel echo lowered to near 5 km MSL. In the developing phase of Storm B, the graupel echo was centered around 4 km MSL (T ~ 0 °C), and then rose to be centered at 5 km MSL by the mature phase of Storm B.

[2] Storm reports were retrieved from the National Climatic Data Center's online Storm Events Database.

[3] The dramatic decline is partially an effect of how the volumetric statistics were calculated. The two storms (A and B) overlapped for about 20 minutes between 0044 and 0052 UTC. Thus, at 0044 UTC the total volume in which statistics are calculated increased to include the newly developing cells. At 0059, Storm A had dissipated such that its volume was no longer included in the statistics calculations, resulting in a dramatic reduction in total volume since the new cells were still quite small. Nonetheless, Storm B rapidly grew and attained volumetric statistics in par with Storm A a short time later.

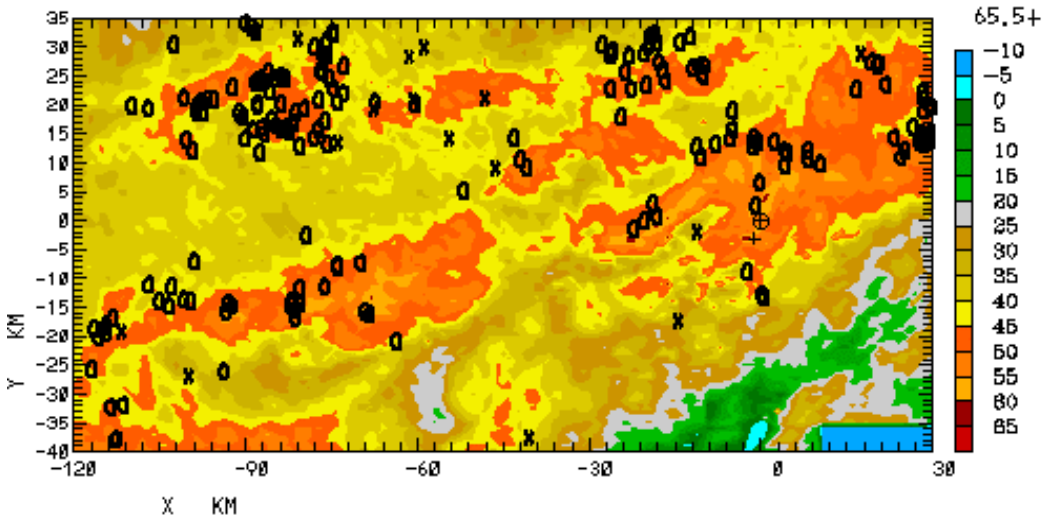

Figure 3. Swath of composite reflectivity from the S-Pol radar accumulated for the period 2314-0213 UTC on 19 June 2000. NLDN cloud-to-ground lightning strikes are overlaid with a black 'O' for negative strikes and a black 'X' for positive strikes. The '⊕' symbol represents the location of the Goodland, Kansas NWS WSR-88D, and the '+' symbol represents the location of maximum reflectivity (65.5 dBZ) for the entire swath.

The total hail echo volume (dominantly small hail) began to slowly increase after 2318 until 2348 UTC, at which point it slightly declined and then rapidly increased to its highest peak around 0020 UTC during Storm A's mature phase (Fig. 4). The hail echo volume (hereafter, hail EV) decreased as Storm A dissipated, but remained fairly high as Storm B began to develop, even during the period of weak updraft in Storm B's developing phase (see Fig. 4). It is possible that Storm B ingested some of Storm A's graupel and hail embryos, allowing it to quickly produce graupel and hail even without having an updraft capable of sustaining large hydrometeor growth from scratch. Hail echo volume in Storm B peaked around 0122, still in the absence of updraft volume greater than 10 m s^{-1}, and then steadily declined until the end of the analysis period (Figs. 4, 5). For the most part, hail EV was only detected near 3 km MSL in the lowest portions of the storm (Fig. 4).

The total lightning flash rate (LFR) was around 10 flashes min^{-1} at the beginning of the analysis period, and rose to near 60 flashes min^{-1} by 0019 UTC during Storm A's mature phase when graupel EV was also at a maximum (Fig. 5). LFR declined for about 10 minutes around 2350 UTC, though a similar decline was not seen in the graupel EV trend (see Fig. 5). Both graupel EV and LFR decreased after 0019 UTC, and then the LFR began to rise again in Storm B around 0052 UTC, when the total hail EV was also beginning to rise again (Figs. 4, 5). Graupel EV rapidly increased a short time later and peaked at the same time as the LFR and hail EV at 0122 UTC, but the graupel EV continued to rise beyond this time, while LFR and hail EV both declined until the end of the period. Considering that this storm system was quite complex and highly evolutionary, it is difficult to interpret the relationships presented in these time series. Nonetheless, the observations indicate that, for the most part, LFR

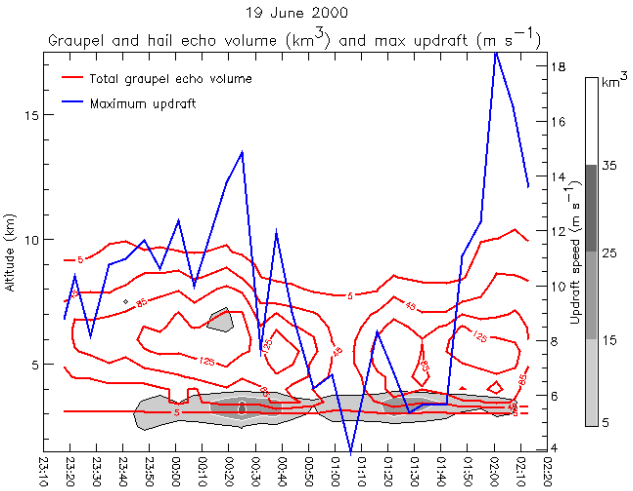

Figure 4. Time-height contours of total graupel echo volume (red contours) and total hail echo volume (gray shaded contours), and maximum updraft time series (values on right axis) for 19 June 2000. For reference, Storm A was observed from 2318-0052 UTC, and Storm B from 0044-0213 UTC.

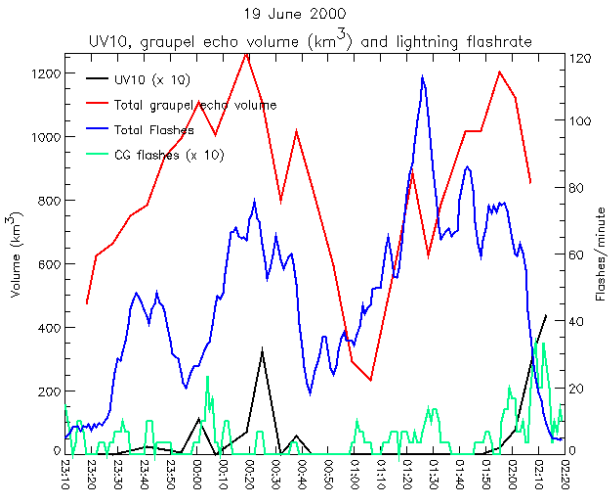

Figure 5. Time series of updraft volume greater than 10 m s^{-1} (multiplied by 10 to fit on left axis), total graupel echo volume (values on left axis), the counted lightning flash rate from the LMA data (values on right axis), and the CG flash rate (multiplied by 10 to fit on right axis) for 19 June 2000.

followed the behavior of graupel EV in Storm A, while LFR seemed to follow the behavior of hail EV in Storm B.

The CG flash rate was relatively low, but steady, throughout Storm A and Storm B, until the demise of Storm B when it approached 4 flashes min^{-1} (Fig. 5). There were, however, a few periods that lacked CG flashes around 0014-0021, during 0040-0100, and near 0140 UTC (Fig. 5). These periods will be discussed in more detail in section 3.3.

3.3 Charge structure

In both Storms A and B, IC flashes were most often observed by the LMA near the core of the storm, initiating both at a height of 8 km MSL and 5 km MSL. Those initiating near 8 km typically propagated upward, with many more LMA sources above the initial height, than below. The IC flashes originating near 5 km MSL typically propagated downward, with the majority of LMA sources below the initial height. This indicates a likely region of positive charge around 8-11km, a main negative charge region around 5-8km, and a lower positive charge layer below 5 km, which is consistent with a "normal tripole" charge structure (illustrated in Fig. 6). The bulk of the LMA sources (most often associated with positive charge) were found between 2-11 km MSL (Fig. 6). In the less electrically active phases of the time series, a dearth of LMA sources near 7 km MSL is visible,

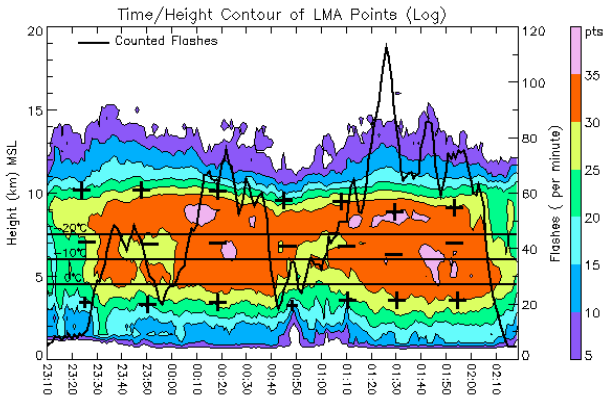

Figure 6. Time-height contours of the total number of LMA sources (color-shaded in logarithmic units) with the total flash rate time series overlaid in black for 19 June 2000. Plus and minus symbols indicate LMA-inferred gross charge structure. Smaller plus symbols indicate a smaller region of lower positive charge, versus a relatively larger region during times with a larger lower plus symbol.

coinciding with the height of the inferred negative charge region (Fig. 6).

Of course, the storm's charge structure was more complex than Figure 6 can demonstrate. Figure 7 therefore illustrates the radar observations and charge structure during three flashes near 0019 UTC in the mature phase of Storm A, which is quite representative of the charge structure in both storms. Low-level CAPPI's of reflectivity and vertical velocity showed that the storm was multicellular, with multiple reflectivity cores, and the low-level updraft was east (ahead) of the advancing storm (Fig. 7a). The core of the storm aloft was mostly graupel, and the three flashes shown in Figure 7 were observed in and near that core of precipitation ice where the majority of charging by ice-ice collisions is presumed to occur. This reinforces the importance of active riming growth in the electrification process. The vertical reflectivity structure of the Storm A (which is similar to that of Storm B) is shown in Figure 7c-d. The main updraft was east (ahead) of the storm and under an overhang in reflectivity. The charge structure in the reflectivity overhang (and main updraft) resembled the "normal dipole" with a main negative charge region centered around 7-8 km MSL, and an upper positive charge region above 9 km MSL (Fig. 7c). In the core of the storm, the "normal tripole" structure can be seen, with the additional lower positive region below 6 km MSL (Fig. 7c). Once more in this projection, it is clear that most of the LMA sources were contained in a

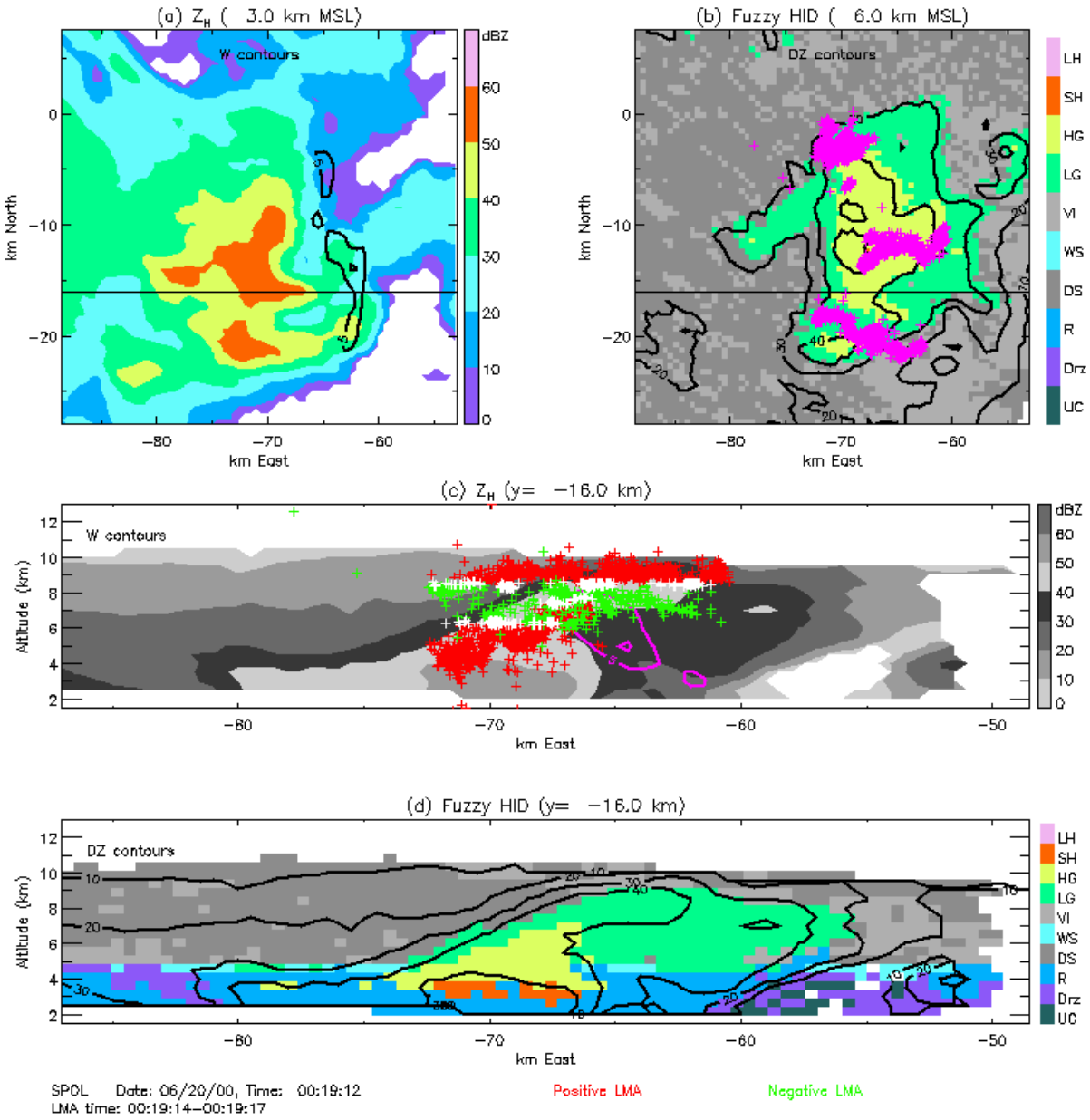

Figure 7. S-Pol radar and LMA data at 0019 on 20 June 2000: a) S-Pol reflectivity at 3 km MSL with updraft contours every 5 m s^{-1}, beginning with 5 m s^{-1}, overlaid in black; b) FHC at 6 km MSL with reflectivity contours every 10 dBZ, beginning with 10 dBZ, overlaid in black; c) Grayscale S-Pol reflectivity at y = -16 km with updraft contours every 5 m s^{-1}, beginning with 5 m s^{-1}, overlaid in pink; and d) FHC at y = -16 km with reflectivity contours every 10 dBZ, beginning with 10 dBZ, overlaid in black. LMA sources from three representative flashes between 00:19:14-00:19:17 are overlaid in pink in (b), and as positive (red), negative (green), or undetermined (white) charge in (c).

region with precipitation ice, such as graupel and small hail (Fig. 7d).

In the LMA data, negative CG lightning flashes usually initiated around 4-5 km MSL and then propagated downward into what is inferred as a lower positive charge region below the main negative region (not shown). The presence of a lower positive charge region involved in the CG flashes supports the idea that a lower charge

region, of opposite sign, is needed to initiate CG lightning toward the ground[4] (Williams et al. 1989, Williams 2001, Mansell et al. 2002, Marshall and Stolzenburg 2002, Wiens et al 2005). No CG flashes were observed near 0019 UTC, rather there were numerous IC discharges between the lower positive and main negative region (see Fig. 5). The lower positive charge region was vertically deeper and larger in area at this time as well. It is possible that since the lower positive charge region was larger in area than it had previously been, and many more IC discharges were detected between the main negative region and the lower positive region, that there was a preference for IC discharges around that time. We presume a similar explanation for the absence of CG flashes near 0140 UTC. Between 0017-0018 UTC, there was also a lightning hole observed in the LMA data (not shown), which has been associated with stronger updrafts and bounded weak echo regions (BWERs) in radar reflectivity CAPPI's (Krehbiel et al. 2000, Wiens et al. 2005). A weak echo region and the core updraft were coincident with this lightning hole (not shown), and it was also during the peak period of the maximum updraft (see Fig. 4). For the period between 0040-0100 UTC, when there was no CG activity, the lower positive region was much less evident and thus the storm exhibited more of a normal dipole structure (see Figs. 5, 6). Again, this supports the notion that in order for there to be CG lightning, a lower charge region is needed.

4. COMPARISON WITH 29 JUNE 2000

The environment on 29 June supported strong, isolated convection with CAPE values of 1254 J kg^{-1} (not shown), compared to only 566 J kg^{-1} on 19 June. The 29 June storm was also a well-organized supercell, with frequent BWERs detected in its reflectivity, associated with strong updrafts as high as 50 m s^{-1} (Fig. 8). Lightning holes were also observed in the regions with BWERs (Wiens et al. 2005). UV10 in 29 June was nearly two orders of magnitude larger than it was in the 19 June storm (Figs. 5, 9). The 29 June storm was much more vertically developed than 19 June, with graupel EV reaching as high as 15 km MSL (Figs. 4, 8). There was also more hail EV in 29 June, with more of a contribution to the total hail EV from large hail, than in 19 June (Fig. 8). Hail EV also was detected throughout a much deeper volume of the storm in 29 June.

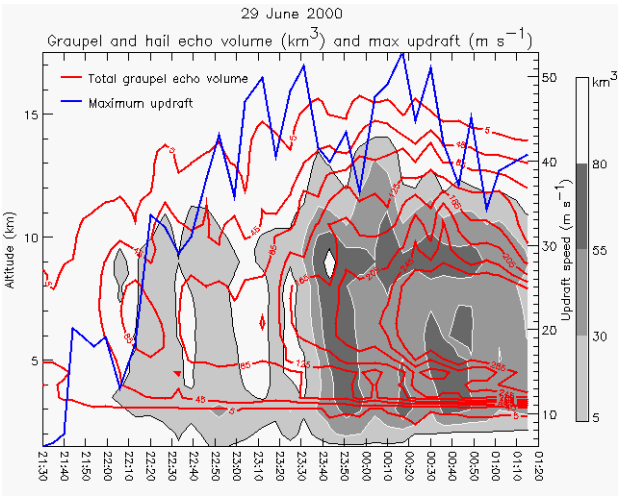

Figure 8. Same as Figure 4 except for 29 June 2000.

The total lightning flash rates in 29 June were on the order of 100s per minute, compared to only 10s per minute in 19 June (Figs. 5, 9). The 29 June storm produced mostly positive cloud-to-ground lightning, while the 19 June storm produced predominantly negative cloud-to-ground lightning, however the CG flash rates were similar between the two storms (Figs. 5, 9). The main factor contributing the opposite polarity of the CG flashes was the charge structure of each storm. The 29 June storm exhibited an "inverted dipole/tripole", with a large region of positive charge in the region where a "normal" storm would have a main negative charge. The bulk of the LMA sources in 29 June were centered around 8 km MSL, where the inferred main positive charge region resided, but also the height at which the main *negative* charge resided in 19 June (Figs. 6, 10). The (positive) CG flashes in 29 June were also documented to occur below a region of lower opposite (negative) charge, which is consistent with the behavior of the CG flashes in 19 June (Wiens et al. 2005).

[4] The few positive CG flashes associated with this storm system initiated around 5 km MSL and propagated upwards into a region of numerous LMA sources (and thus inferred positive charge) just above 5 km MSL, with relatively few LMA sources below yielding an inferred region of lower negative charge below 5 km MSL. This is also consistent with the aforementioned notion that CG lightning needs an oppositely charged lower charge region to initiate CG lightning toward the ground. These CG flashes occurred outside the storm core, and may have been the result of a lowering of the normal dipole charge structure in the storm periphery.

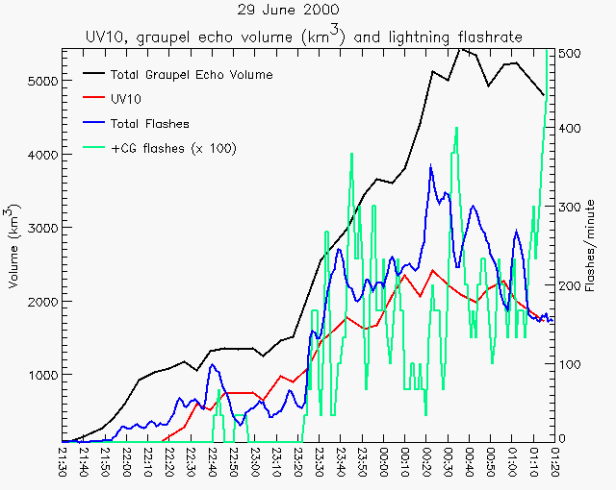

Figure 9. Same as Figure 5 except with positive CG flash rate (x 100) and for 29 June 2000.

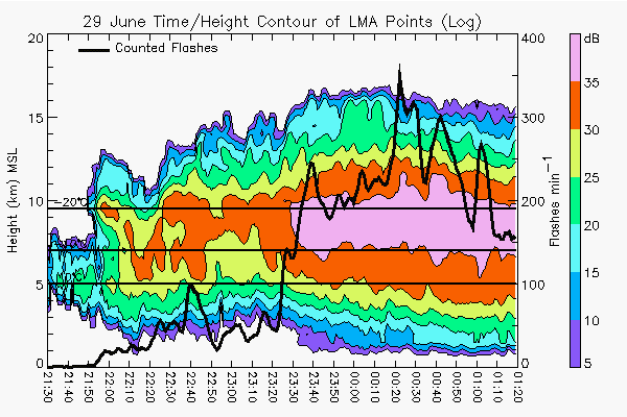

Figure 10. Same as Figure 6 except without inferred charge regions and for 29 June 2000.

5. CONCLUDING REMARKS

The objective of this study was to provide a preliminary discussion of the radar and lightning observations of the 19 June 2000 storm, and compare those to the observations of the well-documented 29 June 2000 supercell. Radar data from CSU-CHILL, NCAR S-Pol, and the Goodland WSR-88D radars were synthesized to determine the three dimensional wind fields, and polarimetric variables from the NCAR S-Pol radar were used to estimate the bulk hydrometeor types within the storm using a fuzzy-logic hydrometeor classification scheme. LMA data were analyzed to determine lightning flash rates and charge structure within the storm.

In summary, the 19 June storm was a shallow, multicellular storm system that produced mostly negative CG lightning and moderate flash rates, while the 29 June storm was an organized positive CG-producing supercell that produced excessive lightning flash rates. Updrafts were stronger and much larger (by two orders of magnitude) in the 29 June supercell than in the 19 June storm. Furthermore, the 19 June storm had very little large hail and much less total hail and graupel EV than 29 June. It was possible, however, that the 19 June storm was ingesting embryos from neighboring cells in the multicellular storm system, which may be how it produced graupel and hail quickly without the obvious storm dynamics to do so. The 19 June storm system exhibited a “normal tripole” charge structure, opposite to the “inverted” structure of 29 June. In agreement with previous studies, we also observed that negative CG flashes in this storm came to ground below a region of lower positive charge, further reinforcing that a lower charge region may be required to initiate CG lightning toward the ground (Williams et al. 1989, Williams 2001, Mansell et al. 2002, Marshall and Stolzenburg 2002, Wiens et al 2005).

Our goal is to better understand why an inverted charge structure occurs, instead of the “normal” structure, and in particular, how the lower charge region develops that is likely the impetus for CG lightning. Clearly, more case studies are needed to further investigate these issues. Our future work includes analysis of another positive CG-producing storm that occurred on 22 June 22 2000 for a comparison with the two cases discussed herein.

Acknowledgements: We would like to thank L. Jay Miller of NCAR for support with the multiple-Doppler analysis. We also thank Dr. Kyle Wiens of Los Alamos National Lab for his assistance and expertise with the LMA analysis and for use of his CDF display software. We also acknowledge Drs. Rob Cifelli, Tim Lang, and Steve Nesbitt for their insightful comments and review of this study. The S-Pol and KGLD data were obtained from NCAR. The CSU-CHILL radar is supported by the National Science Foundation (NSF) under grant ATM-0118021. The LMA data and software were obtained from Dr. Paul Krehbiel, Dr. William Rison, Dr. Ron Thomas, Dr. Tim Hamlin, and Jeremiah Harlin of New Mexico Tech. This research was supported by the NSF Physical Meteorology Program under grant ATM-0309303.

REFERENCES

Carey, L.D., S.A. Rutledge, and W.A. Peterson, 2003: The relationship between severe storm reports and cloud-to-ground lightning polarity in the contiguous United States from 1989-98. *Mon. Wea. Rev*., **131**, 1211-1228.

Cummins, K. L., M. J. Murphy, E. A. Bardo, W. L. Hiscox, R. B. Pyle, and A. E. Pifer, 1998: A combined TOA/MDF technology upgrade of the U.S. National Lightning Detection Network. *J. Geophys. Res*., **103** (D8), 9035–9044.

Kasemir, H. W., 1960: A contribution to the electrostatic theory of lightning discharge. *J. Geophys. Res*., **65**, 1873-1878.

Krehbiel, P.R., R.J. Thomas, W. Rison, T. Hamlin, J. Harlin, and M. Davis, 2000: Lightning mapping observations in central Oklahoma. *EOS*, **81**, 22-25.

Lang, T.J., and co-authors, 2004: The severe thunderstorm electrification and precipitation study. *Bull. Amer. Meteor. Soc,* in press.

Liu, H., and V. Chandrasekar, 2000: Classification of hydrometeors based on polarimetric radar measurements: Development of fuzzy logic and neuro-fuzzy systems and in situ verification. *J. Atmos. Oceanic Technol.*, **17**, 140-164.

MacGorman, D.R., W.D. Rust, P. Krehbiel, E. Bruning, and K. Wiens, 2005: The electrical structure of two supercell storms during STEPS. *Mon. Wea. Rev*., in press.

Mansell, E.R., D.R. MacGorman, C. Ziegler, and J.M. Straka, 2002: Simulated three-dimensional branched lightning in a numerical thunderstorm model. *J. Geophys. Res.*, **107**, doi:10.1029/2000JD00244.

Marshall, T.C., and M. Stolzenburg, 2002: Electrical energy constraints on lightning. *J. Geophys. Res.*, , doi:10.1029/2000JD000024.

Mazur, V. and L. H. Ruhnke, 1993: Common physical processes in natural and artificially triggered lightning. *J. Geophys. Res*., **98**, 12,913-12,930.

Mohr, C.G., L.J. Miller, R.L. Vaughn, and H.W. Frank, 1986: On the merger of mesoscale data sets into a common Cartesian format for efficient and systematic analysis. *J. Atmos. Oceanic. Technol.*, **3**, 143-161.

O'Brien, J.J., 1970: Alternative solutions to the classical vertical velocity problem. *J. Appl. Meteor*., **9**, 197-203.

Rison, W., R. J. Thomas, P. R. Krehbiel, T. Hamlin, and J. Harlin, 1999: A GPS-based three-dimensional lightning mapping system: Initial observations in Central New Mexico. *Geophys. Res. Lett*., **26**, 3573-3576.

Ryzhkov, A.V. and D.S. Zrnic, 1998: Polarimetric rainfall estimation in the presence of anomalous propagation. *J. Atmos. Oceanic Technol.*, **15**, 1320-1330.

Straka, J.M., D.S. Zrnic, and A.V. Ryzhkov, 2000: Bulk hydrometeor classification and quantification using polarimetric radar data: Synthesis of relations. *J. Appl. Meteor*., **39**, 1341-1372.

Tessendorf, S.A., L.J. Miller, K.C. Wiens, and S.A. Rutledge, 2005: The 29 June 2000 supercell observed during STEPS. Part I: Kinematics and microphysics. *J. Atmos. Sci.,* in press.

Thomas, R., P. Krehbiel, W. Rison, J. Harlin, T. Hamlin, and N. Campbell, 2003: The LMA flash algorithm. Abstract C4-23, *Proc. 12th Intl. Conf. On Atmos. Elect*., 655-656, Versailles, France.

Wiens, K.C., S.A. Rutledge, and S.A Tessendorf, 2005: The 29 June 2000 supercell observed during STEPS. Part II: Lightning and charge structure. *J. Atmos. Sci.,* in press.

Williams, E.R., M.E. Weber, and R.E. Orville, 1989: The relationship between lightning type and convective state of thunderclouds. *J. Geophys. Res*., **94**, 13,213-13,220.

Williams, E.R., 2001: The electrification of severe storms. *Severe Convective Storms*, C.A.Doswell III, Ed., *Meteor. Monogr*., No. 50, Amer. Meteor. Soc., 527-561.